Photocatalytic Mineralization of Commercial Herbicides in a Pilot-Scale Solar CPC Reactor: Photoreactor Modeling and Reaction Kinetics Constants Independent of Radiation Field

ARTICLE *in* ENVIRONMENTAL SCIENCE AND TECHNOLOGY · DECEMBER 2009

Impact Factor: 5.33 · DOI: 10.1021/es902004b · Source: PubMed

3 AUTHORS, INCLUDING:

Jose Colina-Márquez
Universidad de Cartagena
20 PUBLICATIONS **109** CITATIONS

SEE PROFILE

Photocatalytic Mineralization of Commercial Herbicides in a Pilot-Scale Solar CPC Reactor: Photoreactor Modeling and Reaction Kinetics Constants Independent of Radiation Field

JOSE COLINA-MÁRQUEZ,[†] FIDERMAN MACHUCA-MARTÍNEZ,[†] AND GIANLUCA LI PUMA*[,‡]

School of Chemical Engineering, Universidad del Valle, Sede Meléndez, Cali, Colombia, and Photocatalysis and Photoreaction Engineering, Department of Chemical and Environmental Engineering, The University of Nottingham, Nottingham, NG7 2RD, U.K.

Received July 6, 2009. Revised manuscript received September 4, 2009. Accepted October 5, 2009.

The six-flux absorption-scattering model (SFM) of the radiation field in the photoreactor, combined with reaction kinetics and fluid-dynamic models, has proved to be suitable to describe the degradation of water pollutants in heterogeneous photocatalytic reactors, combining simplicity and accuracy. In this study, the above approach was extended to model the photocatalytic mineralization of a commercial herbicides mixture (2,4-D, diuron, and ametryne used in Colombian sugar cane crops) in a solar, pilot-scale, compound parabolic collector (CPC) photoreactor using a slurry suspension of TiO_2. The ray-tracing technique was used jointly with the SFM to determine the direction of both the direct and diffuse solar photon fluxes and the spatial profile of the local volumetric rate of photon absorption (LVRPA) in the CPC reactor. Herbicides mineralization kinetics with explicit photon absorption effects were utilized to remove the dependence of the observed rate constants from the reactor geometry and radiation field in the photoreactor. The results showed that the overall model fitted the experimental data of herbicides mineralization in the solar CPC reactor satisfactorily for both cloudy and sunny days. Using the above approach kinetic parameters independent of the radiation field in the reactor can be estimated directly from the results of experiments carried out in a solar CPC reactor. The SFM combined with reaction kinetics and fluid-dynamic models proved to be a simple, but reliable model, for solar photocatalytic applications.

Introduction

Solar heterogeneous photocatalysis based on TiO_2 has been proposed as an environmentally friendly method for the treatment of water and wastewater contaminated with priority pollutants. Herbicides are among the most common priority pollutants in agricultural and surface waters which are resistant to conventional water treatment methods. A large variety of herbicides have been treated successfully by photocatalytic oxidation in laboratory and pilot-scale studies (*1*−*6*). However, for a subsequent application of this technology at larger scale, it becomes necessary to use reliable and robust models which can describe the kinetics of herbicides removal in a predictable way. This requires the use of mathematical models of the photocatalytic treatment process. Currently, large scale photocatalytic treatment plants for research and development are most often designed by experience rather than by using rigorous scientific principles.

One of the most complex tasks in photocatalytic reactor modeling is the estimation of the local volumetric rate of photon absorption (LVRPA) which in turns depends on the spatial distribution of the radiant field in the photoreactor. This process can become more difficult when solar radiation is the source of photons due to the geographical variability and the nature of propagation (diffuse or direct) of solar radiation.

Many studies in the literature have been aimed to the modeling of lab-scale photoreactors operated with artificial UV radiation and under very controlled conditions (*7*−*12*). The models reported are either very simplistic or rigorous (*13*−*17*), and consequently they may be difficult to be applied to the analysis of complex reactor geometries in pilot plants. The simplistic approach, often reported in the literature, which neglect the modeling of the radiation field in the photoreactor, usually applies to the photoreactor configuration under study and to the operating conditions and radiation source used. The kinetic parameters obtained with this approach cannot be used for scale-up since they are not independent of the photon absorption effect and the LVRPA. The more rigorous approach (*11*−*13, 18*−*20*) involves the solution of the radiative transfer equation (RTE) in the reactor, and yields kinetic parameters, independent of the radiation field in the photoreactor which can be used for scale-up. However, the mathematical analysis needed to solve the RTE can be demanding, especially in complex reactors. Li Puma et al. (*8*) and Brucato et al. (*21*) reported a model that could estimate the LVRPA analytically through the solution of differential photon balances, with a simple procedure which solved the RTE considering probabilities to the photon scattering directions. This model, named Six-Flux Absorption-Scattering Model (SFM) solves the RTE without abandoning the essentials features of the rigorous approach. The SFM was successfully applied to annular photoreactors modeling with single (*8*) and multicomponent (*10*) systems of herbicides and to flat heterogeneous reactors (*21*).

Bandala et al. (*22*) compared the efficiency of several pilot-scale, solar photoreactor geometries (compound parabolic collector (CPC), tubular, parabolic through concentrator and V-shaped collector) for the degradation of common herbicides in a slurry suspension of TiO_2, and concluded that the CPC configuration was the most efficient. It consists of a tubular reactor with two involute reflectors as shown in Figure 1. In this configuration, both direct and diffuse components of solar radiation are utilized to irradiate the photoreactor. The development of a rigorous model for the degradation of pollutants in a solar CPC photocatalytic reactor is currently lacking in the literature.

In this work, the SFM combined with reaction kinetics and fluid-dynamics models was used to model the photocatalytic mineralization of a commercial herbicides mixture (2,4-D, diuron, and ametryne used in Colombian sugar cane crops) in a solar, pilot-scale, CPC photoreactor. The solar

* Corresponding author phone: +44(0)1159514170; Fax: +44(0)1159514115; e-mail: gianluca.li.puma@nottingham.ac.uk.
[†] Universidad del Valle.
[‡] The University of Nottingham.

10.1021/es902004b CCC: $40.75
Published on Web 11/02/2009

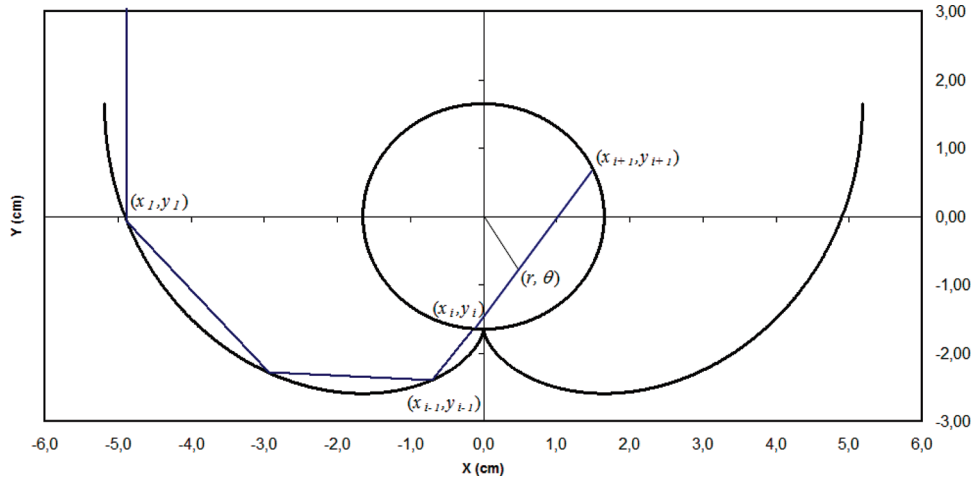

FIGURE 1. Reflected ray trajectory in a CPC.

radiation parameters of the experimental site were estimated to obtain the annual averaged diffuse and direct UV intensities. The ray-tracing technique was used to calculate the coordinates and the direction of the photon flux corresponding to the reflected direct and diffuse component of solar radiation. The complex radiation field and the volumetric distribution of the LVRPA in the CPC reactor was estimated by the SFM combined with the ray-tracing technique. As a result, the kinetic parameters derived from the fitting of the model to the experimental results were independent of the radiation field in the reactor and therefore more universally applicable to the design and scale-up of solar CPC reactors for sustainable environmental remediation.

Modeling of a Solar CPC Photoreactor for Oxidation of a Herbicides Mixture.

Herbicides Mineralization Kinetics. The application of herbicides to crops in most cases demands the use of a mixture of several active ingredients and additives. As a result, the TOC measurement becomes a suitable choice for following the mineralization of these compounds. Although the TOC concentration is a global parameter, several studies have shown that in most cases the TOC removal by photocatalysis follows pseudo first-order kinetics (*17, 22*−*25*) and an apparent Langmuir−Hinshelwood (L−H) rate equation. The L−H rate law must include an explicit dependence from the photonic effect, represented by the LVRPA, in order to determine kinetic parameters which are independent of reactor geometry and radiation field (*10*). Toepfer et al. (*10*), proposed a rate law for a mixture of herbicides as follows:

$$-r_{\mathrm{j}} = k_{\mathrm{r,j}}(\mathrm{LVRPA})^{m}\frac{K_{\mathrm{j}}C_{\mathrm{j}}}{1+\sum_{\mathrm{j}}K_{\mathrm{j}}C_{0,\mathrm{j}}} \tag{1}$$

where $k_{\mathrm{r,j}}$ is the kinetic constant, and K_{j} is the binding constant associated to the adsorption of the herbicides onto the catalyst surface. The exponent m depends on the efficiency of electron−hole formation and recombination at the catalyst's surface and takes a value between 0.5 and 1 providing the reaction is kinetically controlled. Since eq 1 applies to a multicomponent solution of herbicides and include the effect of reaction intermediates (*9, 10*), the concentration C_{j} can be replaced by the global parameter TOC since all components in solution (herbicides and intermediates) undergo photocatalytic oxidation to yield mineralization products.

The average intensity of UV solar radiation varies with the time of the year, geographical location and with the atmospheric conditions, as a result, the photocatalytic treatment time was standardized based on a constant solar radiation intensity of 30 W/m^2 (*2, 4, 26, 27*) which corresponds to the average intensity achieved in a clear sunny day. The time $t_{30\mathrm{W}}$, was calculated as follows:

$$t_{30\mathrm{W},i} = t_{30\mathrm{W},i-1} + \Delta t_{\mathrm{n}}\frac{\mathrm{UV}}{30}\cdot\frac{V_{\mathrm{R}}}{V_{\mathrm{T}}} \tag{2}$$

$$\Delta t_{\mathrm{n}} = t_i - t_{i-1} \tag{3}$$

where Δt_{n} is the time interval between sampling, UV is the average UV solar intensity (W/m^2) during the sampling time interval, and V_{R} and V_{T} are the reactor and total (the volume of liquid in the entire system) liquid volumes, respectively.

This approach allows the development of a model which is independent of geographical location or the time of the year of the experiments.

SFM Parameters. The SFM was used to estimate the rate of UV solar energy absorbed at each point in the reaction space (LVRPA). The following assumptions were made: Uniform distribution of photocatalytic particles in the suspension and invariant optical characteristics; negligible absorption of energy by the fluid or the reactor walls; solar UV radiation absorbed by the photocatalyst (TiO_2) of wavelength between 295 and 384 nm (anatase band gap); constant reflectivity of the reflector surface.

The optical parameters considered in the SFM include the scattering albedo ω of the TiO_2 suspension:

$$\omega = \frac{\sigma}{\sigma+\kappa} \tag{4}$$

where σ and κ are the spectral-averaged specific mass scattering and absorption coefficients, respectively. The sum $(\sigma + \kappa)$ is the extinction coefficient. σ and κ depend on the wavelength of the energy spectrum, and they have been reported (*28*) for several types of TiO_2-based photocatalysts, including P-25 used in this study. The spectral-averaged absorption and scattering coefficients were calculated from the solar radiation spectrum I_λ (*29*) as follows:

$$\sigma = \frac{\int_{\lambda_{\min}}^{\lambda_{\max}}\sigma_\lambda I_\lambda \mathrm{d}\lambda}{\int_{\lambda_{\min}}^{\lambda_{\max}} I_\lambda \mathrm{d}\lambda} \tag{5}$$

$$\kappa = \frac{\int_{\lambda_{min}}^{\lambda_{max}} \kappa_\lambda I_\lambda d\lambda}{\int_{\lambda_{min}}^{\lambda_{max}} I_\lambda d\lambda} \quad (6)$$

with the upper and lower integration limits defined by the maximum (385 nm for TiO_2 anatase; note that the rutile phase is generally considered to be photocatalytically inactive) and the minimum (295 nm) wavelength of solar radiation which have energy higher than the band gap of the photocatalyst (3.2 eV).

The probabilities of the forward, backward, and side scattering (p_f, p_b, and p_s) were used to estimate the corrected scattering albedo (*21*):

$$a = 1 - \omega p_f - \frac{4\omega^2 p_s^2}{(1 - \omega p_f - \omega p_b - 2\omega p_s)} \quad (7)$$

$$b = \omega p_b + \frac{4\omega^2 p_s^2}{(1 - \omega p_f - \omega p_b - 2\omega p_s)} \quad (8)$$

$$\omega_{corr} = \frac{b}{a} \quad (9)$$

The values of p_f, p_b, and p_s were 0.11, 0.71 and 0.045, respectively, for a diffusively reflecting, large sphere, phase function (*21*).

The other SFM parameters, i.e., optical thickness τ, apparent optical thickness τ_{app}, extinction length $\lambda_{\omega corr}$, and γ were estimated from ref *10*:

$$\tau = (\sigma + \kappa) c_{cat} \delta \quad (10)$$

$$\tau_{app} = a\tau\sqrt{1 - \omega_{corr}^2} \quad (11)$$

$$\lambda_{\omega corr} = \frac{1}{a(\sigma + \kappa) c_{cat}\sqrt{1 - \omega_{corr}^2}} \quad (12)$$

$$\gamma = \frac{1 - \sqrt{1 - \omega_{corr}^2}}{1 + \sqrt{1 - \omega_{corr}^2}} \exp(-2\tau_{app}) \quad (13)$$

where c_{cat} is the catalyst concentration and δ is the estimated reactor thickness in the direction of the incident photon flux entering the reactor wall.

The ray-tracing technique was used to compute the direction of the reflected photon flux, and the coordinates of the points where the light ray intercepted the circular section of the reactor or the collector surface (Figure 1). The photon flux pathway was calculated from simple geometry:

$$\delta = \sqrt{(x_{i+1} - x_i)^2 + (y_{i+1} - y_i)^2} \quad (14)$$

where the *i*-subscript corresponds to the number of direction changes that a photon undergoes before reaching the reactor wall (Figure 1). For simplification purposes, the possible change of direction due to the refraction at the reactor wall was neglected.

Incident Solar Radiation Intensity. The following considerations were made for estimating the incident radiation intensity I_0: Constant solar radiation intensity along the

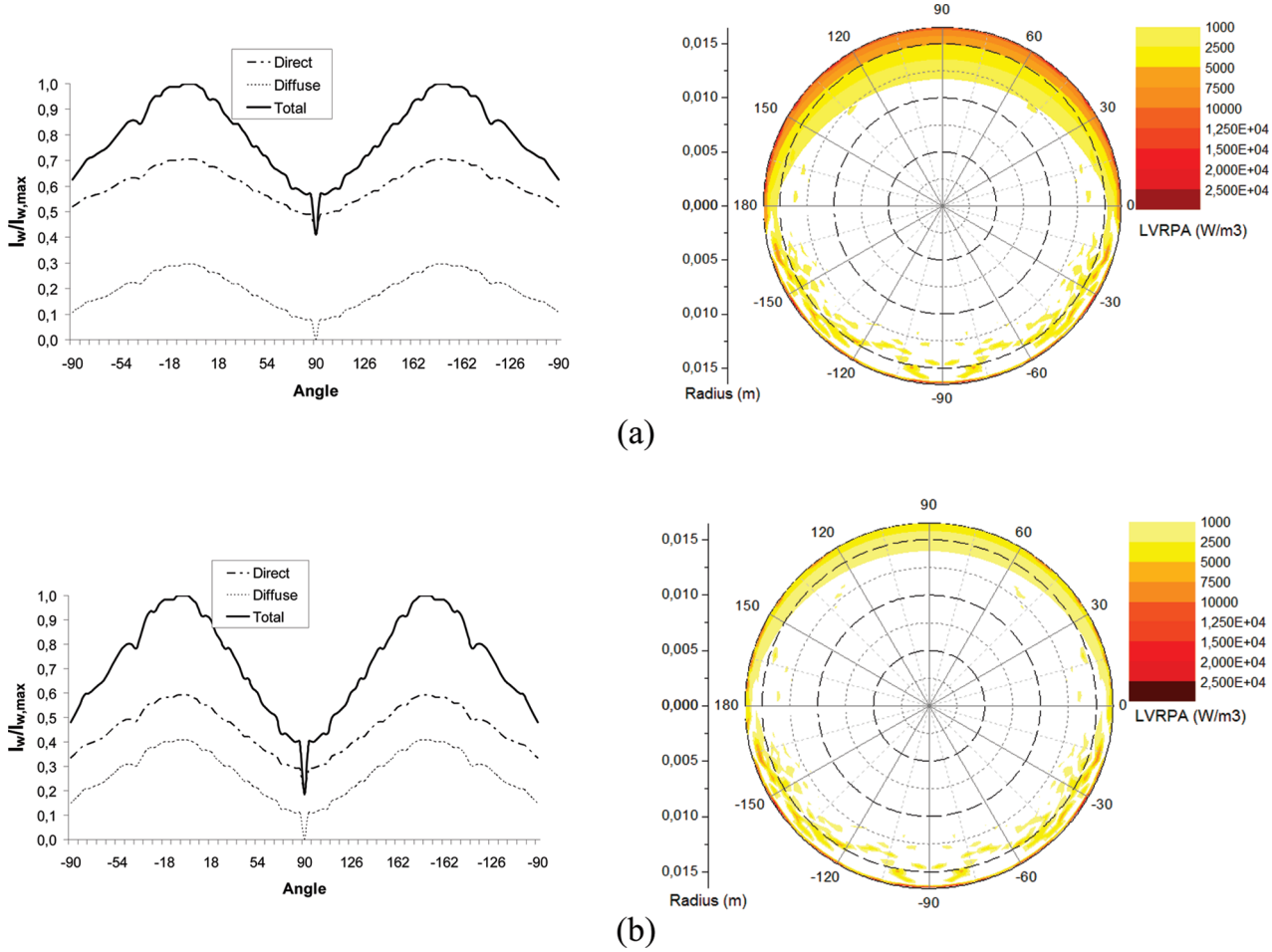

FIGURE 2. LVRPA distribution in the CPC photoreactor. (a) sunny day; (b) cloudy day.

reactor axial direction; the total solar radiation intensity $I_{0,\mathrm{Total}}$ fixed at 30 W/m^2, according to the previous standardization of the irradiation time (eq 2); constant ratio of diffuse to direct solar radiation; 75% UV transmittance through the clouds (data shows that it varies from 60 to 90% (*31*) although it depends on the cloud type).

The ratio of diffuse-to-direct radiation depends on the geographical location and the time of the year of the experiments (*30*). The first parameter to be computed for the estimation of this ratio was the year fraction η (eq 15) expressed as an angle:

$$\eta = \frac{2\pi d_{\mathrm{n}}}{365} \tag{15}$$

where d_{n} corresponds to the day of the year, (e.g., $d_{\mathrm{n}} = 1$ for January the first) followed by the declination angle ϖ (eq 16) and the solar angular hour, h_{a} (eq 17):

$$\varpi = 0.006918 - 0.399912\cos\eta + 0.070257\sin\eta - 0.006758\cos 2\eta + 0.000907\sin 2\eta - 0.002697\cos 3\eta + 0.00148\sin 3\eta \tag{16}$$

$$h_{\mathrm{a}} = \arccos(-\tan\phi\tan\varpi) \tag{17}$$

The value of the global solar radiation H_0, which is the total intensity estimated for a perfect sunny clear day, was estimated from the following equations (*30*):

$$E_0 = 1 + 0.033\cos\eta \tag{18}$$

$$H_0 = (24/\pi)SE_0\sin\phi\sin\varpi \cdot [h_{\mathrm{a}} - \tan(h_{\mathrm{a}})] \tag{19}$$

where E_0 is the eccentricity correction factor and S is a solar constant (S = 1.367 KWh/m^2). The cloudiness ratio K_{C} (eq 20) and the diffuse-to-total radiation ratio, H_{d}/H (eq 21) were computed from the H_0 value and the received radiation H in the location of interest as follows:

$$K_{\mathrm{C}} = \frac{H}{H_0} \tag{20}$$

$$\frac{H_{\mathrm{d}}}{H} = \begin{cases} 0.99 \text{ for } K_{\mathrm{C}} \le 0.17 \\ 1.188 - 2.272K_{\mathrm{C}} + 9.473K_{\mathrm{C}}^2 - 21.856K_{\mathrm{C}}^3 + 14.648K_{\mathrm{C}}^4 \text{ for } 0.17 < K_{\mathrm{C}} \le 0.80 \end{cases} \tag{21}$$

Equations 18−21 are valid for the total solar radiation (*30*). The UV diffuse-to-total radiation ratio and the direct UV radiation intensity were estimated considering that the UV energy in the interval (295−384 nm) was 4.1% of the total solar radiation and considering 75% transmittance through the clouds. It follows:

$$\frac{I_{0,\mathrm{diff}}}{I_{0,\mathrm{Total}}} = \frac{(0.041)(0.75)H_0 - (1 - H_d/H)(0.041)H}{(0.041)(0.75)H_0} \tag{22}$$

$$I_{0,\mathrm{direct}} = I_{0,\mathrm{Total}} - I_{0,\mathrm{diff}} \tag{23}$$

The direct and diffuse UV intensities were determined by taking $I_{0,\mathrm{Total}}$, = 30 W/m^2 (*2, 4, 26, 27*).

Estimation of the LVRPA. The LVRPA estimated from the SFM in the direction of traveling of the incident photon flux, r_{p} is (*8*):

$$\mathrm{LVRPA} = \frac{I_0}{\lambda_{\omega\mathrm{corr}}\omega_{\mathrm{corr}}(1-\gamma)}[(\omega_{\mathrm{corr}} - 1 + \sqrt{1-\omega_{\mathrm{corr}}^2})e^{-r_p/\lambda_{\omega\mathrm{corr}}} + \gamma(\omega_{\mathrm{corr}} - 1 - \sqrt{1-\omega_{\mathrm{corr}}^2})e^{r_p/\lambda_{\omega\mathrm{corr}}}] \tag{24}$$

I_0 in eq 24 corresponds to the components of solar radiation reaching the reactor walls, either direct radiation or diffuse radiation. The direct component of solar UV radiation, $I_{0,\mathrm{direct}}$, was estimated from the geometry of the pipe assuming that the photon flux entered the reactor space vertically (Supporting Information (SI) Figure S-2a). SI Figure S-2a also shows the direction of the direct radiation reflected by the solar collector.

The diffuse component of solar UV radiation, $I_{0,\mathrm{diff}}$, was calculated by randomization of the directions of the diffuse photon flux as shown in SI Figure S-2b.

Snell's law of specular materials was used to estimated the intensity of both direct and diffuse radiation reflected by the collector surface reaching the reactor (*32*):

$$I_{0,\mathrm{reflected}} = I_0\psi^g \tag{25}$$

where ψ is the material reflectance and g is the number of consecutive reflections of the ray (Figure 1).

Finally, the overall $\mathrm{LVRPA}_{\mathrm{r},\theta}$, at a specific location (r, θ) in the reaction space, was the sum of the LVRPA estimated from each radiation component (direct, diffuse, and the reflected radiation by these two components).

Fluid dynamic model and material balance. Beside the reaction kinetics and radiation balance, the modeling of the CPC photoreactor requires a fluid dynamic model and the description of the material balances on each of the reacting species. Pilot-scale CPC photoreactors using slurry suspensions of TiO_2, are usually operated in the turbulent flow regime ($Re > 10000$) (*3, 33, 34*) to avoid mass transfer limitations and catalyst sedimentation. Assuming steady-state operation, a fully developed fluid velocity profile, constant physical and rheological properties of the suspension and negligible axial dispersion, the radial profile of fluid velocity (SI Figure S-1) was estimated as follows (*35*):

$$\frac{v_z}{v_{z,\max}} = \left(1 - \frac{r}{R}\right)^{1/n} \tag{26}$$

where R is the reactor radius and n is a parameter which can be determined by the following expression (*35*):

$$n = 0.41\sqrt{\frac{8}{f}} \tag{27}$$

where f is the friction factor. The maximum and average fluid velocities $v_{z,\max}$ and $v_{z,\mathrm{average}}$ were calculated from

$$v_{z,\mathrm{average}} = \frac{Q}{\pi R^2} \tag{28}$$

$$\frac{v_{z,\max}}{v_{z.average}} = \frac{(n+1)(2n+1)}{2n^2} \tag{29}$$

where Q is the liquid flow rate.

With the fluid-dynamic model established, the mass balance for the reacting species (herbicides and intermediates) represented by the TOC, in a photocatalytic reactor operated at steady-state and in batch mode with recirculation reduces to

$$Q\frac{\mathrm{dTOC}_{r,\theta}}{\mathrm{d}V_{\mathrm{R}}} = -\frac{k_{\mathrm{I}}K_{\mathrm{I}}\mathrm{TOC}_{\mathrm{r},\theta}}{(1 + K_{\mathrm{I}}\mathrm{TOC}_0)}(\mathrm{LVRPA})_{r,\theta}^m \tag{30}$$

where V_{R} is the volume of the reactor exposed to solar radiation.

The right-hand side of eq 30 corresponds to the L−H type rate law (eq 1) for a single compound with C_j and $C_{0,j}$ replaced by TOC and TOC_0, the initial TOC concentration of the herbicide mixture. Since the LVRPA varies in both the radial and the angular directions, the local reaction rate varies with space. The boundary conditions to solve eq 30 are

$$z = 0,\ \mathrm{TOC} = \mathrm{TOC}^{\mathrm{in}} \tag{31}$$

where TOC^{in} corresponds to the inlet TOC concentration to the reactor in a given time. Separating the variables and integrating, it follows:

$$\mathrm{TOC}_{r,\theta}^{\mathrm{out}} = \exp\left[\ln(\mathrm{TOC}^{\mathrm{in}}) - \frac{k_{\mathrm{T}}}{v_z(1 + K_1\mathrm{TOC}_0)}\int_0^L (\mathrm{LVRPA})_{r,\theta}^m \mathrm{d}z\right] \tag{32}$$

where L is total length of the photoreactor. The TOC concentration at the reactor outlet in each pass is:

$$\mathrm{TOC}_{\mathrm{average}}^{\mathrm{out}} = \frac{\int_0^{2\pi}\int_0^R r v_z \mathrm{TOC}_{r,\theta}^{\mathrm{out}} \mathrm{d}r\mathrm{d}\theta}{Q} \tag{33}$$

The above reactor analysis neglects radial mixing of the fluid. Under turbulent flow conditions this assumption is inaccurate and complete radial mixing may be assumed. Therefore, the entire reactor was discretized to a very large number of differential reactor volumes (ΔV_R), and eqs 30−33 were solved iteratively for a differential reactor length (ΔL) until the entire reactor volume V_R was considered.

Following the method described in Li Puma et al. (*8*) for a recirculation reactor systems with a total volume V_T, the number of passes through the reactor in a given time t_{30W} was

$$n_{\mathrm{pass}} = \frac{Qt_{30\mathrm{W}}}{V_{\mathrm{R}}} \tag{34}$$

and the change in TOC concentration change per each pass was

$$\mathrm{TOC}_{i+1}^{\mathrm{in}} = \frac{\mathrm{TOC}_i^{\mathrm{in}}(t - V_{\mathrm{R}}/Q)(V_{\mathrm{T}} - V_{\mathrm{R}}) + \mathrm{TOC}_i^{\mathrm{out}}V_{\mathrm{R}}}{V_T} \quad \text{with } i = 1, 2, 3...n_{\mathrm{pass}} \tag{35}$$

where i is the number of passes.

Materials and Methods

SI Figures S-3 and S-4 shows a schematic representation of the pilot-scale CPC photoreactor used in this study and the solar pilot plant setup. It consisted of ten Duran glass tubes (1200 mm in length, 32 mm o.d., 1.4 mm wall thickness), supported by a metal structure. The high reflectance (ψ = 0.85) involute aluminum CPC surfaces were located underneath the glass tubes as shown in Figure 1.

The reactor was operated in a recirculation mode using a 40 L recycle feed tank and a recycling centrifugal pump ($^1/_2$ hp of nominal power) that delivered 30.2 L/min. The flow rate was measured by a calibrated flowmeter. The pipeline and accessories used in the pilot plant were made of PVC, 1 in. diameter.

A herbicides mixture used in the Colombian sugar cane crops was synthetically prepared, from a stock solution, using commercial formulations of 2,4-D (2,4-dichlorophenoxyacetic acid), diuron, and ametryne. This mixture was prepared and diluted with tap water to simulate the concentration of wastewater typically produced in the rinsing of empty herbicides containers. The concentration of each herbicide was under their solubility value. The following commercial products were diluted in 1 L of tap water: 10 mL of Profiamina (720 g/L of 2,4-D as dimethylamine salt), 2 g of Karmex (70% w/w of diuron), 20 mL of Igram (99% w/w of ametryne) 1 mL of Inex-A (Cosmoagro) and 0.67 g of Cosmo-Aguas (Cosmoagro). The last two components are common proprietary surfactants and pH regulator additives used in the formulation of the herbicides mixture for sugar cane crops. The mixture was stirred for 30 min before taking aliquots due to the low solubility of diuron. We diluted 20, 35, and 70 mL aliquots of the stock solution in 20 L of tap water inside the recycle-feed tank. The pH was adjusted with NaOH (Merck).

TABLE 1. Solar Radiation for Cali, Colombia (2008)

month	H (KWh/m^2)	H_0 (KWh/m^2)	K_C	H_d/H
January	4.75	9.6515	0.4922	0.6183
February	4.75	10.1292	0.4689	0.6602
March	5.25	10.4565	0.5021	0.5999
April	4.75	10.3768	0.4578	0.6797
May	4.25	9.9768	0.4260	0.7320
June	4.75	9.6604	0.4917	0.6192
July	5.25	9.7351	0.5393	0.5288
August	4.75	10.1042	0.4701	0.6582
September	4.75	10.3604	0.4585	0.6785
October	4.75	10.2041	0.4655	0.6663
November	4.25	9.7557	0.4356	0.7166
December	4.25	9.4715	0.4487	0.6951
Averages	4.71	9.9902	0.4714	0.6544

The catalyst added to the solution was TiO_2, Aeroxide P-25 supplied by Degussa (primary particle size, 20−30 nm by TEM; specific surface area 52 m^2 g^{-1} by BET; composition 78% anatase and 22% rutile by X-ray diffraction).

The TOC concentration was followed with a Shimadzu 5050A TOC analyzer. The solution pH was measured with an AB15 pH-meter from Fisher Scientific. The intensity of the UV solar radiation in the 295−380 nm interval and the corresponding accumulated energy with time was measured with an Acadus S50 UV radiometer. The dissolved oxygen was monitored by a DOB-343 oxygen meter.

The experimental tests were carried out at the Solar Photocatalysis Laboratory of the Universidad del Valle, located in Cali (Colombia) (3° 29′ N latitude) (SI Figure S-5). The pilot-scale photoreactor was operated from early March to mid April 2009. The experiments were carried out under dry and partly cloudy and under sunny weather conditions. In a typical experimental run, the initial pH of the working solution was set to 9.0 (the optimal pH which yielded the faster mineralization rate) and the catalyst concentration was 0.6 g/L. The circulation flow rate was held at 30.2 L/min to ensure turbulent flow (Reynolds number = 19420; SI). The slurry was recirculated for 30 min in the dark to approach adsorption equilibrium between the substrate, the solid catalyst and the walls of the apparatus. The system was subsequently irradiated with 35 W·h/m^2 of accumulated solar UV energy. Samples were collected every 2.5 W·h/m^2, they were filtered through 0.45 μm Nylon Millipore filter and analyzed for TOC content. The filter was not found to retain organic matter. The slurry was aerated naturally by the contact of the return stream with atmospheric air in an artificial waterfall flowing over the feed-recycle tank. The dissolved oxygen concentration was kept above 60% of saturation at the observed temperature of the liquid (29.3 ± 2.1 °C).

Experimental Validation of the Model

Solar Radiation Parameters. The solar radiation parameters were averaged from the monthly data reported in the Solar Atlas of Colombia (*30*) for Cali. The results (Table 1) calculated

TABLE 2. SFM Optical Parameters

parameter	
specific mass absorption coefficient κ, $m^2\ kg^{-1}$	1295.75
specific mass scattering coefficient σ, $m^2\ kg^{-1}$	174.75
scattering albedo, ω, dimensionless	0.88
SFM parameter, *a*, dimensionless	0.87
SFM parameter, *b*, dimensionless	0.66
scattering corrected albedo, ω_{corr}, dimensionless	0.75
extinction length, $\lambda_{0,\ \omega corr}$, m	1.98×10^{-3}

using the equations presented earlier show steady solar conditions along the year (see also SI Table S-1). Consequently, the adoption of average solar parameters was justified. The steadiness of the solar conditions is advantageous for large-scale applications of solar photocatalysis in tropical regions. The diffuse component of the total solar radiation from eq 22 was found to be 78.3%. This suggests that solar photoreactor design must be aimed at improving the utilization of the diffuse component of the total solar radiation.

Estimation of LVRPA. The optical parameters were calculated from the properties of the catalyst combined with the solar radiation spectrum (*29*) (eqs 5−6). The results are presented in Table 2 and SI Table S-2. The extinction coefficient ($\sigma + \kappa$) was measured according to the method in ref *28*, under the prevailing conditions of mixing in the reactor (note that the optical characteristics of the catalyst may change due to agglomeration/disintegration as a result of changes of pH and solute composition). Using the specific absorption coefficient for TiO_2 (Degussa P-25) reported in (*28*) the average specific absorption coefficient was calculated from eq 6. Table 2 shows the SFM parameters from eqs. (7,8,9,12) other than, τ_{app} and γ, which varied with the direction of the incident radiation entering the reactor.

The angular distribution of the diffuse and direct solar radiation intensities at the outer wall of the photoreactor and the angular and radial distribution of the LVRPA for a cross section of the solar CPC photoreactor are shown in Figure 2, for both sunny and cloudy days. The incident solar radiation flux did not vary along the axial direction *z*. In a sunny day (Figure 2a) the largest values of the LVRPA is located in the upper region of the tube as a result of a larger component of direct solar radiation. A sharp radial gradient in the LVRPA is observed. Conversely in a cloudy day (Figure 2b), the angular distribution of the LVRPA is more uniform, due to a larger component of diffuse incident radiation, but the observed LVRPA are lower. These results confirmed the importance of using reflecting collectors that aim at improving the distribution and usage of UV solar radiation, especially in geographical locations with significant diffuse radiation.

Kinetic Parameters. The experimental data obtained were processed to standardize the illumination time as proposed in eqs 2−3. Combining the rate law (eq 1) (replacing Cj with TOC) with the material balance in the batch recirculation reaction system, which has total volume (V_T) and reactor volume (V_r), it follows

$$V_T \frac{dTOC}{dt_{30W}} = -\frac{K_1 TOC}{1 + K_1 TOC_0} k_T \int_{V_r} (LVRPA)^m dV_r \quad (36)$$

Rearranging eq 36, the reaction kinetic constant and the order of the reaction with respect to the LVRPA were determined from the initial rate of TOC removal:

$$\frac{1}{V_T\left(-\frac{dTOC}{dt}\right)_{t=0}} = \frac{1}{k_T K_1 \int_{V_r} (LVRPA)^m dV_r}\left(\frac{1}{TOC_0}\right) + \frac{1}{k_T \int_{V_r} (LVRPA)^m dV_r} \quad (37)$$

The kinetic parameters for the L−H model of the eq 1 were estimated from the linear regression of the reciprocal values of initial rates and initial concentrations as shown in Figure 3. The values of k_T and K_1 were estimated from the intercept and slope of the fitting line. It follows:

$$k_T = \frac{1}{(1.2 \times 10^4)(327.57) \int_{V_R} (LVRPA)^{0.5} dV_R} = 1.1564 \times 10^{-7} \text{mol L}^{-1}\text{s}^{-1}\text{W}^{-0.5}\text{m}^{1.5} \quad (38)$$

$$K_1 = \frac{(286411.55)(1.2 \times 10^4)}{327.57} = 1.05 \times 10^7 \text{L mol}^{-1} \quad (39)$$

where 1.2×10^4 ppm·mol^{-1}·L is the conversion factor from ppm to mol L^{-1}. The coefficient *m* in the LVRPA was taken to be 0.5 since the irradiation intensities were higher than those reported in ref *10* for herbicides photocatalytic oxidation. The above constants apply to the studied mixture with its specific composition (initial TOC in the range 25−50 ppm) and under the prevailing conditions of mixing (catalyst dispersion and agglomeration) in the reactor. Nonetheless, the kinetic parameters reported here are independent of reactor geometry and radiation field, therefore, these results can be used for scale-up purposes. It should be noted that the kinetic parameter k_T is essentially an adjustable parameter that can accommodate changes in the adopted scattering phase function and optical properties of the suspension.

Figure 4 shows a satisfactory fit of the TOC degradation curves by the model presented in this work for three different initial TOC concentrations (Figure 4a) and for a sunny and a cloudy day (Figure 4b). The rate of TOC degradation was faster in a sunny day due to larger values of LVRPA in the reactor (Figure 4a). The complex radiation field and the volumetric distribution of the LVRPA in the CPC reactor was estimated by the SFM combined with the ray-tracing technique. As a result, the kinetic parameters derived from the fitting of the model to the experimental results were independent of the radiation field in the reactor and therefore more universally applicable to the design and scale-up of solar CPC reactors compared to semiempirical rate laws based on the incident flux or on the overall radiation absorbed in the photoreactor.

The SFM combined with reaction kinetics and fluid-dynamic models proved to be a simple, but reliable model, for solar photocatalytic applications. The removal of her-

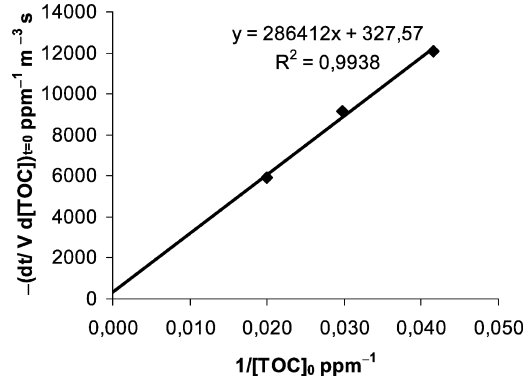

FIGURE 3. Linear regression analysis for estimation of the L−H parameters.

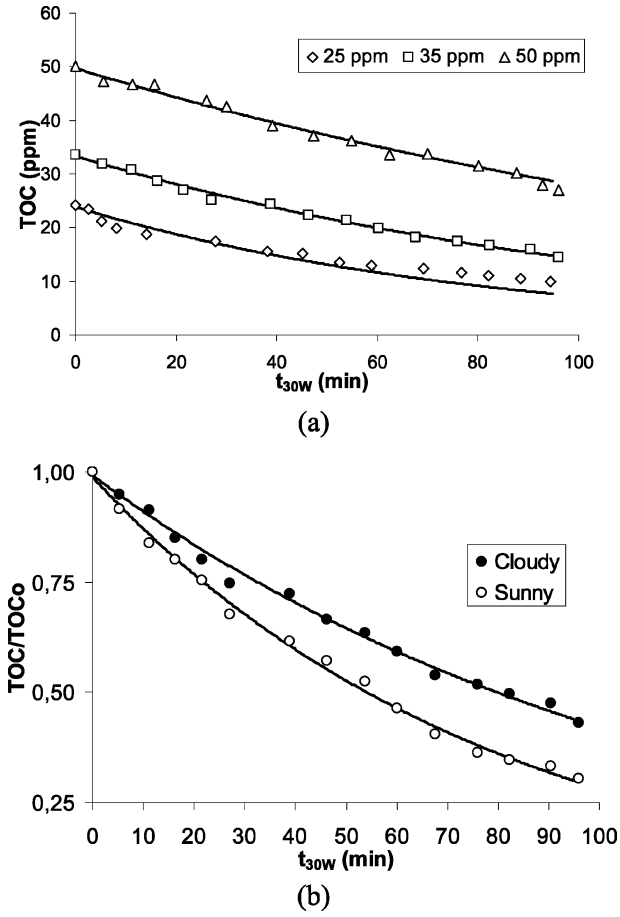

FIGURE 4. TOC degradation (SFM vs experimental). (a) $I_{average}$ = 10.0 W/m^2; (b) TOC_0 = 35 ppm. (●) $I_{average}$ = 10 W/m^2, H_d/H = 0.65 (○) $I_{average}$ = 22 W/m^2 H_d/H = 0.26.

bicides from contaminated water can be effectively carried out in CPC solar photoreactors designed using the model presented in this work. The complexity of catalyst separation and reuse/recycle can be solved by using a cross-flow filtration unit or possibly a simple sedimentation tank if catalyst agglomeration occurs.

New photocatalysts with wider absorption spectrum of solar radiation (e.g., nonmetal-doped TiO_2) could allow wider use of photocatalytic detoxification technologies for environmental remediation. The modeling approach presented here can easily accommodate the use of these new materials, after suitable measurement of their optical properties and the estimation of the spectral-averaged absorption and scattering coefficients (eqs 5−6).

Acknowledgments

Financial support from the Universidad del Valle (Grant 2565), Colciencias (Grant 110647922029) and from NATO (Grant: CBP.EAP.SFPP 982835) is gratefully acknowledged. Machuca-Martínez and Colina-Márquez thank Colciencias for the financial support during their Ph.D. studies. Finally, a special acknowledgement to Ch. Eng. Augusto Arce for carrying out the experimental tests.

Nomenclature

a	SFM parameter, dimensionless
b	SFM parameter, dimensionless
c_{cat}	catalyst concentration, kg m^{-3}
d_n	day of the year, d
E_0	eccentric correction factor, dimensionless
f	friction factor, dimensionless
g	number of successive reflections, dimensionless
h_a	solar angular hour, radians
H	total solar radiation, kWh m^{-2}
H_0	global solar radiation, kWh m^{-2}
H_d	diffuse solar radiation, kWh m^{-2}
I	UV radiation intensity, W m^{-2}
k_T	kinetic constant, mol L^{-1} s^{-1} W$^{-0.5}$ m$^{1.5}$
K_I	binding constant, L mol^{-1}
K_C	cloudiness factor, dimensionless
L	reactor length, m
LVRPA	local volumetric rate of photon absorption, W m^{-3}
m	reaction order with respect to the LVRPA, dimensionless
n	parameter of velocity profile for turbulent regime, dimensionless
n_{pass}	number of passes of the fluid through the reactor space, dimensionless
p_b	probability of backward scattering, dimensionless
p_f	probability of forward scattering, dimensionless
p_s	probability of side scattering, dimensionless
Q	flow rate, m^3 s^{-1}
r	radial coordinate, m
r_p	auxiliary coordinate in the photon flux direction, m
R	reactor radius, m
S	solar radiation parameter, 1.367 kWh m^{-2}
t	time, s
t_{30W}	standardized 30 W time, s
TOC	TOC concentration, mol L^{-1}
v	velocity, m s^{-1}
V	volume, m^3
x	horizontal coordinate, m
y	vertical coordinate, m
z	axial coordinate, m

Greek letters

δ	reactor thickness, m
ϕ	latitude, radians
γ	SFM parameter, dimensionless
η	year fraction, dimensionless
κ	specific mass absorption coefficient, m^2 kg^{-1}
λ	radiation wavelength, nm
θ	polar coordinate, radians
σ	specific mass scattering coefficient, m^2 kg^{-1}
τ	optical thickness, dimensionless
ϖ	declination angle, radians
ω	scattering albedo, dimensionless
ψ	reflectance,dimensionless

Subscripts

app	apparent
average	average
corr	corrected
diff	diffuse radiation
direct	direct radiation
max	maximum
min	minimum
r	radial coordinate
reflected	reflected radiation
R	reactor
total	total radiation
T	Total
z	axial coordinate
0	relative to incident radiation, or initial condition
λ	radiation wavelength
θ	angular coordinate
corr	corrected albedo

Superscripts

in	reactor inlet
out	reactor outlet

Supporting Information Available

Figure S-1. Velocity profile for turbulent regime. Figure S-2. (a) Ray-tracing of solar direct radiation; (b) Ray-tracing of solar diffuse radiation. Figure S-3. Pilot-scale solar CPC photoreactor. Figure S-4. Schematics of solar pilot plant setup. Figure S-5. Solar radiation map for January for the experimental site. Table S-1. Solar radiation parameters for Cali (Colombia, 2008). Table S-2. Optical properties of TiO_2 suspension. This material is available free of charge via the Internet at http://pubs.acs.org.

Literature Cited

(1) Malato, S.; Caceres, J.; Fernandez-Alba, A. R.; Piedra, L.; Hernando, M. D.; Aguera, A.; Vial, J. Photocatalytic treatment of diuron by solar photocatalysis: Evaluation of main intermediates and toxicity. *Environ. Sci. Technol.* **2003**, *37*, 2516–2524.

(2) Malato, S.; Blanco, J.; Fernandez-Alba, A. R.; Aguera, A. Solar photocatalytic mineralization of commercial pesticides: Acrinathrin. *Chemosphere* **2000**, *40*, 403–409.

(3) Malato, S.; Blanco, J.; Vidal, A.; Richter, C. Photocatalysis with solar energy at a pilot-plant scale: An overview. *Appl. Catal., B* **2002**, *37*, 1–15.

(4) Malato, S.; Blanco, J.; Vidal, A.; Fernández, P.; Cáceres, J.; Trincado, P.; Oliveira, J. C.; Vincent, M. New large solar photocatalytic plant: set-up and preliminary results. *Chemosphere* **2002**, *47*, 235–240.

(5) Haque, M. M.; Muneer, M.; Bahnemann, D. W. Semiconductor-mediated photocatalyzed degradation of a herbicide derivative, chlorotoluron, in aqueous suspensions. *Environ. Sci. Technol.* **2006**, *40*, 4765–4770.

(6) Dai, K.; Peng, T. Y.; Chen, H.; Zhang, R. X.; Zhang, Y. X. Photocatalytic degradation and mineralization of commercial methamidophos in aqueous titania suspension. *Environ. Sci. Technol.* **2008**, *42*, 1505–1510.

(7) Fu, J.; Ji, M.; Zhao, Y.; Wang, L. Kinetics of aqueous photocatalytic oxidation of fulvic acids in a photocatalysis-ultrafiltration reactor (PUR). *Sep. Purif. Technol.* **2006**, *50*, 107–113.

(8) Li Puma, G.; Khor, J. N.; Brucato, A. Modeling of an annular photocatalytic reactor for water purification: Oxidation of pesticides. *Environ. Sci. Technol.* **2004**, *38*, 3737–3745.

(9) Gora, A.; Toepfer, B.; Puddu, V.; Li Puma, G. Photocatalytic oxidation of herbicides in single-component and multicomponent systems: Reaction kinetics analysis. *Appl. Catal., B* **2006**, *65*, 1–10.

(10) Toepfer, B.; Gora, A.; Li Puma, G. Photocatalytic oxidation of multicomponent solutions of herbicides: Reaction kinetics analysis with explicit photon absorption effects. *Appl. Catal., B* **2006**, *68*, 171–180.

(11) Satuf, M. L.; Brandi, R. J.; Cassano, A. E.; Alfano, O. M. Modeling of a flat plate, slurry reactor for the photocatalytic degradation of 4-chlorophenol. *Int. J. Chem. Reactor Eng.* **2007**, *5*, A59.

(12) Satuf, M. L.; Brandi, R. J.; Cassano, A. E.; Alfano, O. M. Photocatalytic degradation of 4-chlorophenol: A kinetic study. *Appl. Catal., B-* **2008**, *82*, 37–49.

(13) Brandi, R. J.; Citroni, M. A.; Alfano, O. M.; Cassano, A. E. Absolute quantum yields in photocatalytic slurry reactors. *Chem. Eng. Sci.* **2003**, *58*, 979–985.

(14) Cassano, A. E.; Alfano, O. M. Reaction engineering of suspended solid heterogeneous photocatalytic reactors. *Catal. Today* **2000**, *58*, 167–197.

(15) Imoberdorf, G. E.; Irazoqui, H. A.; Cassano, A. E.; Alfano, O. M. Quantum efficiencies in a multi-annular photocatalytic reactor. *Water Sci. Technol.* **2007**, *55*, 161–166.

(16) Mahmoodi, N. M.; Arami, M.; Limaee, N. Y.; Tabrizi, N. S. Kinetics of heterogeneous photocatalytic degradation of reactive dyes in an immobilized TiO_2 photocatalytic reactor. *J. Colloid Interface Sci.* **2006**, *295*, 159–164.

(17) Qamar, M.; Muneer, M.; Bahnemann, D. Heterogeneous photocatalysed degradation of two selected pesticide derivatives, triclopyr and daminozid in aqueous suspensions of titanium dioxide. *J. Environ. Manage.* **2006**, *80*, 99–106.

(18) De Los Milagros Ballari, M.; Alfano, O. M.; Cassano, A. E. Photocatalytic degradation of dichloroacetic acid. A kinetic study with a mechanistically based reaction model. *Ind. Eng. Chem. Res.* **2009**, *48*, 1847–1858.

(19) Marugán, J.; van Grieken, R.; Cassano, A. E.; Alfano, O. M. Scaling-up of slurry reactors for the photocatalytic oxidation of cyanide with TiO_2 and silica-supported TiO_2 suspensions. *Catal. Today* **2009**, *144*, 87–93.

(20) Zalazar, C. S.; Romero, R. L.; Martín, C. A.; Cassano, A. E. Photocatalytic intrinsic reaction kinetics I: Mineralization of dichloroacetic acid. *Chem. Eng. Sci.* **2005**, *60*, 5240–5254.

(21) Brucato, A.; Cassano, A. E.; Grisafi, F.; Montante, G.; Rizzuti, L.; Vella, G. Estimating radiant fields in flat heterogeneous photoreactors by the six-flux model. *AIChE J.* **2006**, *52*, 3882–3890.

(22) Bandala, E. R.; Estrada, C. Comparison of solar collection geometries for application to photocatalytic degradation of organic contaminants. *J. Sol. Energy Eng.* **2007**, *129*, 22–26.

(23) Bizani, E.; Fytianos, K.; Poulios, I.; Tsiridis, V. Photocatalytic decolorization and degradation of dye solutions and wastewaters in the presence of titanium dioxide. *J. Hazard. Mater.* **2006**, *136*, 85–94.

(24) Lhomme, L.; Brosillon, S.; Wolbert, D.; Dussaud, J. Photocatalytic degradation of a phenylurea, chlortoluron, in water using an industrial titanium dioxide coated media. *Appl. Catal., B* **2005**, *61*, 227–235.

(25) Tanaka, K.; Reddy, K. Photodegradation of phenoxyacetic acid and carbamate pesticides on TiO_2. *Appl. Catal., B* **2002**, *39*, 305–310.

(26) Hincapiè, M.; Maldonado, M. I.; Oller, I.; Gernjak, W.; Saìnchez-Peìrez, J. A.; Ballesteros, M. M.; Malato, S. Solar photocatalytic degradation and detoxification of EU priority substances. *Catal. Today* **2005**, *101*, 203–210.

(27) McLoughlin, O. A.; Fernaǹdez Ibàñez, P.; Gernjak, W.; Malato Rodriguez, S.; Gill, L. W. Photocatalytic disinfection of water using low cost compound parabolic collectors. *Sol. Energy* **2004**, *77*, 625–633.

(28) Satuf, M. L.; Brandi, R. J.; Cassano, A. E.; Alfano, O. M. Experimental method to evaluate the optical properties of aqueous titanium dioxide suspensions. *Ind. Eng. Chem. Res.* **2005**, *44*, 6643–6649.

(29) *Standard Tables for Reference Solar Spectral Irradiance*, ASTM G173; ASTM International: West Conshohocken, PA, 2003.

(30) IDEAM. *Apéndice A in: Atlas De Radiación Solar De Colombia*, 1st ed.; Ministerio del Medio Ambiente: Bogota, 2005; p 133.

(31) IDEAM. *Apéndice a in: Atlas De Radiación Solar De Colombia*, 1st ed.; Ministerio del Medio Ambiente: Bogota, 2005; pp 133−145.

(32) Siegel, R., Howell, J. R. *Thermal Radiation Heat Transfer*, 3rd, ed.; Hemisphere: Washington, DC, 1992.

(33) Blanco-Galvez, J.; Malato-Rodriguez, S.; Peral, J.; Sanchez, B., Cardona, A. I. Diseño de reactores para fotocatálisis: Evaluación comparativa de las distintas opciones. In *Eliminación de Contaminantes por Fotocatálisis Heterogénea*; Blesa, M., Ed.; CYTED: Madrid, 2001; pp243−266; ISBN: 987−43−3809−1. Available at http://www.cnea.edu.ar/xxi/ambiental/CYTED/17cap11.pdf.

(34) Malato, S.; Blanco, J.; Maldonado, R.; Fernández, P.; Alarcón, D.; Collares-Pereira, M.; Farinha, J.; Correia de Oliveira, J. Engineering of solar photocatalytic collectors. *Sol. Energy* **2004**, *77*, 513–524.

(35) Bird, R., Stewart, W., Lightfoot. E. *Transport Phenomena*, 2nd, ed.; John Wiley and Sons: New York, 2002.

ES902004B